ACS Catalysis

pubs.acs.org/acscatalysis

Research Article

Probing Active-Site Relocation in Cu/SSZ-13 SCR Catalysts during Hydrothermal Aging by In Situ EPR Spectroscopy, Kinetics Studies, and DFT Calculations

Yani Zhang, Yue Peng, Junhua Li,* Kyle Groden, Jean-Sabin McEwen, Eric D. Walter,* Ying Chen, Yong Wang, and Feng Gao*

Cite This: *ACS Catal.* 2020, 10, 9410−9419

Read Online

ACCESS | Metrics & More | Article Recommendations | Supporting Information

ABSTRACT: Cu/SSZ-13 selective catalytic reduction catalysts display activity loss after mild hydrothermal aging without support degradation or loss of isolated Cu cation content. By applying electron paramagnetic resonance spectroscopy to compare hydrated, dehydrated, and NH_3-saturated catalysts before and after hydrothermal aging, as well as density functional theory calculations, it is found that hydrothermal aging induces Cu relocation, leading to stronger Cu−support interactions. This is particularly evidenced by ZCuOH conversion to Z_2Cu, which leads to the generation of a structure with two Cu(II) cations positioned in a double six-membered ring prism. These two Cu(II) ions have a separation of ∼3.90 Å as derived by EPR analysis, which agrees well with our DFT-based model. The Cu(II) cations that do not undergo such dramatic changes also appear to stay closer to framework windows as evidenced by the overall increased anisotropy during EPR measurements. In situ EPR measurements under SCR conditions demonstrate that, in comparison to the fresh catalyst, a higher percentages of Cu species stay as Cu(II) in the aged catalyst. This suggests that the reduction half-cycle of the SCR redox, i.e., Cu(II) → Cu(I), becomes slower for the hydrothermally aged catalyst.

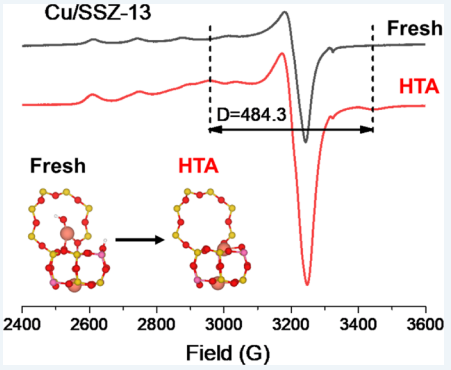

KEYWORDS: *SCR, Cu/SSZ-13, reaction kinetics, EPR, in situ spectroscopy*

1. INTRODUCTION

Copper-exchanged SSZ-13 (Cu/SSZ-13) has drawn much attention as an active and selective catalyst for the selective catalytic reduction of nitrogen oxides with ammonia (NH_3-SCR), which is an important process for diesel engine exhaust after-treatment systems.[1−5] The elucidation of the chemical nature of the active Cu sites (i.e., their location, coordination environment, and activity) in this catalyst has been highly informative thanks to continuous research efforts by numerous researchers over the past decade.[3,5] On the basis of Rietveld refinement of variable-temperature X-ray diffraction (XRD) studies, Fickel and Lobo[6] first proposed that copper stays exclusively as exchanged, isolated Cu^{2+} ions in this catalyst, and they are located just outside the windows of six-membered rings (6MR) coordinated to three zeolite lattice oxygen atoms. This motif has been duplicated in double 6MR prisms of the SSZ-13 lattice in this work using density functional theory (DFT) and is shown in Figure 1 (specifics of calculations are given later). Korhonen et al.[7] later proposed on the basis of SCR reaction tests, ultraviolet−visible (UV−vis), and Cu K-edge X-ray absorption near edge structure (XANES) spectroscopy studies that these isolated Cu^{2+} ions are the active sites for NH_3-SCR. However, subsequent investigations by a few research groups found experimental evidence at variance with such a simple structure model. For example, Kwak et al.[8] first suggested the presence of two different cationic Cu sites in Cu/SSZ-13 based on differences in (1) their reducibility measured by temperature-programmed reduction with H_2 (H_2-TPR) and (2) their perturbation of the support framework vibrations measured by diffuse reflectance infrared Fourier transform spectroscopy (DRIFTS). Giordanino et al.[9] utilized FTIR, UV−vis, and electron paramagnetic resonance (EPR) spectroscopies to compare Cu/SSZ-13 with other Cu/zeolites and first reported the presence of Cu−OH moieties in Cu/SSZ-13. Nam and collaborators also reported the presence of two types of Cu ions and first demonstrated their hydrothermal stability difference.[10] More recent studies, particularly synchrotron-based spectroscopic investigations and DFT simulations, have led to the current general agreement that two isolated Cu(II) ions, i.e., Z_2Cu and ZCuOH (Z represents a framework negative charge), are indeed present in Cu/SSZ-13, with their energetically most

Received: April 7, 2020
Revised: June 29, 2020
Published: June 30, 2020

https://dx.doi.org/10.1021/acscatal.0c01590
ACS Catal. 2020, 10, 9410−9419

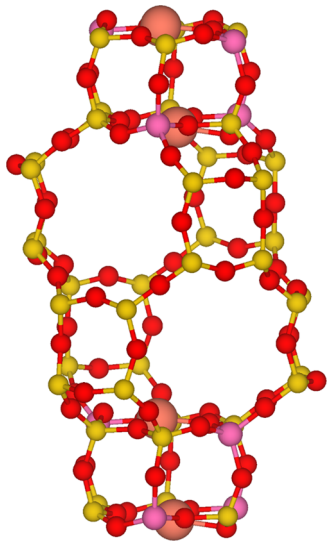

Figure 1. Model of the SSZ-13 structure with Cu^{2+} ions sited in the planes of the double 6-membered rings. The copper (Cu), oxygen (O), aluminum (Al) and silicon (Si) atoms are the orange, red, pink and yellow spheres, respectively.

favorable extra framework locations near windows of 6MR and 8MR, respectively.[11−15] These structures are schematically shown in Figure S1. At low temperatures (<250 °C), these Cu ions are readily solvated by H_2O and/or NH_3. Upon solvation, they migrate away from framework windows into CHA cages; these solvated and isolated Cu moieties have been suggested to be active sites in low-temperature NH_3-SCR (<250 °C).[16,17]

The population of the two Cu(II) sites in a particular Cu/SSZ-13 catalyst depends on multiple factors, particularly catalyst composition (Si/Al and Cu/Al ratios) and treatment history (including, e.g., degreening and hydrothermal aging). The higher thermodynamic stability of Z_2Cu than ZCuOH has been successfully used to explain many experimental findings, for example, the population of Z_2Cu prior to ZCuOH during ion-exchange and the conversion of ZCuOH to Z_2Cu during hydrothermal aging.[18−21] The derivation of such conclusions, however, requires the development of methods that can be readily utilized to quantify Z_2Cu and ZCuOH. H_2-TPR has been quite extensively used to distinguish these two sites, noting that ZCuOH reduces at lower temperatures than Z_2Cu.[10,22,23] However, quantification can be complicated by the presence of CuO_x clusters and autoreduction of ZCuOH during sample pretreatment prior to TPR. Very recently, Tronconi and collaborators have elegantly developed titration protocols using NO, NO_2, and NH_3 to quantify these two sites.[24] The best spectroscopic method that can be used to quantify these two Cu(II) moieties is EPR spectroscopy, which has been widely used to characterize copper-exchanged zeolites because of its excellent spectral resolution and sensitivity.[9,25−29] Isolated Cu^{2+} (d^9) has one unpaired electron, which allows ready observation by EPR. The correlations between spin Hamiltonian parameters and hyperfine coupling constants allow elucidation of the coordination environments surrounding the spectroscopically observed copper ions.

In terms of Z_2Cu and ZCuOH quantification by EPR, Mossin and collaborators reported an important discovery in 2014 that ZCuOH becomes EPR-silent upon dehydration due to a so-called "pseudo Jahn−Teller effect".[27] This discovery conveniently allows both Z_2Cu and ZCuOH to be measured using fully hydrated samples but only Z_2Cu to be measured using dehydrated samples, making quantification of these two sites straightforward. Using this methodology, Song et al.[18] were able to precisely quantify various Cu species of a Cu/SSZ-13 catalyst (Si/Al = 12, Cu loading = 2.1 wt %) hydrothermally aged at different temperatures, which allowed the authors to verify (1) the conversion of ZCuOH to Z_2Cu at mild aging temperatures (<700 °C) and (2) the conversion of ZCuOH to CuO_x clusters at harsh aging temperatures (>700 °C). During this latter study, the authors also discovered some new Cu EPR features that appeared in dehydrated, hydrothermally aged (HTA) samples. The series of EPR spectra are replotted here in Figure 2a,b. As is

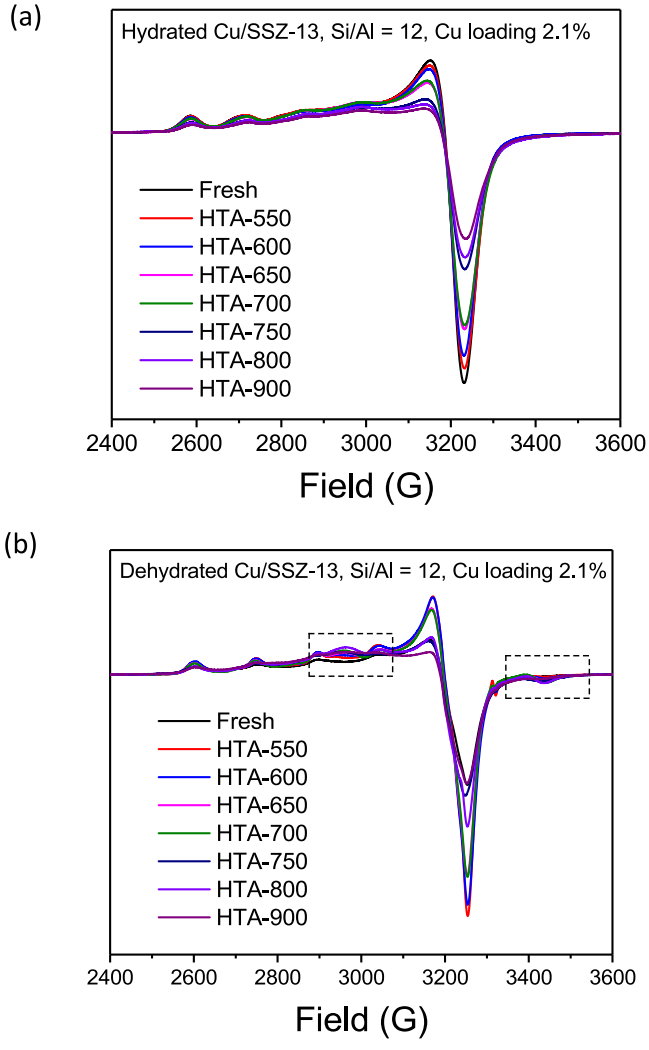

Figure 2. EPR spectra for (a) hydrated and (b) dehydrated fresh and HTA Cu/SSZ-13 catalysts. Spectra were acquired at −150 °C. Sample dehydration was achieved by flowing dry He through the samples at 250 °C for 1 h. Note that these spectra were replotted from Reference 18.

clearly shown in Figure 2a, the EPR signal intensity decreases with increasing aging temperature for the fully hydrated samples as a result of the loss of isolated Cu(II) cations; however, all samples display highly similar spectral lineshapes suggesting a similar nature and local environments of H_2O-solvated Cu(II) species in different samples. In contrast, in addition to the "normal" Z_2Cu signals, new "positive" (~2960 G, highlighted with a dashed rectangle) and "negative" features (~3440 G, highlighted with a dashed rectangle) appear in the hyperfine and

https://dx.doi.org/10.1021/acscatal.0c01590
ACS Catal. 2020, 10, 9410−9419

high-field regions, respectively, for samples that were dehydrated (Figure 2b), with the intensities of these new features increasing with increasing aging temperature. The spectroscopic origin of the positive and negative appearances of these features is due to the fact that continuous-wave (CW) EPR spectra are presented in derivative mode - these peaks represent a splitting of the maximum. In their original publication, Song et al.[18] were unable to explain the nature of Cu(II) sites that give rise to these new EPR features. To our knowledge, such EPR signals have not been reported by others either. In the present study, we used a new Cu/SSZ-13 catalyst to reproduce this phenomenon and provided detailed (in situ) EPR analysis and DFT calculations to elucidate why such new EPR signals only appear in hydrothermally aged catalysts and how SCR performance is influenced by the corresponding structural changes of Cu/SSZ-13.

2. EXPERIMENTAL AND COMPUTATIONAL PROCEDURES

2.1. Synthesis of Fresh and Hydrothermally Aged Cu/SSZ-13 Catalysts. The SSZ-13 zeolite with a Si/Al ratio of 6 was synthesized by a hydrothermal method described elsewhere.[14,18] The Cu/SSZ-13 catalyst was prepared by sequential aqueous phase ion exchanges in the following way. The synthesized Na/SSZ-13 support was first ion-exchanged with an NH_4NO_3 solution to obtain NH_4/SSZ-13. After dispersing 10 g of zeolite in 100 mL of 0.1 M NH_4NO_3 solution, exchange was conducted at 80 °C for 4 h under stirring. The process was repeated three times to ensure complete Na^+ removal. Subsequently, 1 g of NH_4/SSZ-13 was dispersed in 100 mL of 0.01 M $CuSO_4$ solution; upon adjustment of the pH to ∼3.0 by adding drops of 0.1 M HNO_3, exchange was also conducted at 80 °C for 4 h under stirring. Finally, the solid was recovered by centrifugation and thoroughly washed with deionized water before drying and calcination in air at 550 °C for 4 h. The sample thus prepared is denoted as the "fresh" catalyst. A portion of the fresh catalyst was hydrothermally aged in flowing wet air containing 10% water vapor at 600 °C for 20 h, which is denoted as the "HTA" catalyst. The Cu content of the catalyst is 1.21 wt %, measured via inductively coupled plasma atomic emission spectroscopy (ICP-AES) that was performed at Galbraith Laboratories (Knoxville, TN, United States). This gives rise to a Cu/Al ratio of ∼0.1.

2.2. H_2-TPR Experiments. Temperature-programmed reduction with H_2 (H_2-TPR) experiments were conducted using a Micromeritics AutoChem II analyzer. Typically, ∼100 mg of catalyst stored under ambient laboratory conditions was used for each measurement. TPR was carried out in 5% H_2/Ar with a flow rate of 30 mL/min. The temperature was ramped linearly from ambient to 1000 °C at 10 °C/min and held at 1000 °C for 30 min. H_2 consumption was monitored with a TCD detector. Quantification was based on H_2-TPR of a Ag_2O standard chemical provided by Micromeritics.

2.3. In Situ EPR Experimental Details. A flow cell was created by immobilizing 10 mg of Cu/SSZ-13 sample between two quartz wool plugs in a 3 mm quartz tube with a 0.5 mm hole in the bottom. The loaded tube was fixed in an outer 5 mm sealed quartz tube with an inlet and outlet, which makes it a plug-flow reaction system. Four independent gas lines with Brooks mass flow controllers were connected to a diversion valve just outside the magnet of the EPR spectrometer. Switching the valve allowed the mixed gases into the reactor system within seconds. The system pressure drop was monitored in real time. The gas mixture contained 360 ppm NH_3, 360 ppm NO, 10% O_2, and balanced with N_2. The total gas flow was kept at 100 mL/min, corresponding to a gas hourly space velocity of ∼400,000 h^{-1}. The sample was heated using a Bruker ER 4131 continuous flow temperature control system. The EPR spectra were collected with a Bruker E580 X-band spectrometer continuously during the experiment, with the magnetic field swept between 2400 and 3600 G in 83 s with a time constant of 83 ms. The field was modulated at 100 kHz and with an amplitude of 5 G, and the microwave frequency was typically 9.3 GHz with a power of 0.2 mW.

2.4. SCR Reaction Tests with Online Product Analysis. Because our in situ EPR system was not routinely equipped with an analyzer for SCR product analysis, the SCR reaction was also conducted "ex situ" using our plug-flow reaction unit equipped with an online MKS MultiGas 2030 FTIR gas analyzer.[18] To mimic the SCR reaction conditions of in situ EPR, the same reactant composition and space velocity of ∼400,000 h^{-1} was used as for the EPR experiments: 90 mg of catalyst was used, and the total gas flow was kept at 900 mL/min. NO and NH_3 conversions were calculated using the formulas reported elsewhere.[30,31]

2.5. Computational Methods. All calculations were performed using spin-polarized Kohn−Sham DFT implemented within the Vienna Ab initio Simulation Package (VASP).[32,33] Plane waves were used as basis sets for the valence Kohn−Sham states (cutoff energy of 520 eV) and were mapped onto the true all-electron states using the projected augmented wave (PAW) method to accurately account for core electrons during all calculations.[34] The PAW potential data sets released by VASP developers in 2012 were used in this work. Electronic exchange and correlation were treated at the generalized gradient approximation level using the Perdew−Burke−Ernzerhof (PBE) functional.[35] Self-consistent field cycles were considered to be converged once energy changes between subsequent iterations were below 10^{-4} eV. Geometry optimizations (where the unit cell was held fixed) were considered complete once forces on all atomic degrees of freedom were below 0.04 eV/Å.

To model SSZ-13 using ab initio techniques, we chose to use the hexagonal (36 T, 72 O) instead of the rhombohedral unit cell (12 T, 24 O) for our calculations.[36,37] Due to the size of the unit cell (approximately $a = b = 13.72$ Å and $c = 14.95$ Å), only the gamma point was used to sample the first Brillouin zone. This specific cell contains a double six-membered-ring (6MR) prism, which was critical to model the experimentally observed phenomena. The cell itself was optimized when four Si atoms were substituted with Al and charge-compensated by Cu within this pair of rings. This was done by scanning over several cell volumes, allowing the cell shape and atomic degrees of freedom to relax at each chosen volume. For each cell volume, two relaxations were performed followed by a final single point calculation from which the energy was taken to aid in determining the minimum energy cell volume and shape at our previously described level of theory.[36,37] When four Al atoms are replaced with four Si atoms and charge compensated with two Cu(II) cations, this procedure gives an equilibrium volume of approximately 2486 $Å^3$ ($a = 13.87$ Å, $b = 13.66$ Å, $c = 15.24$ Å, $\alpha = 90.3°$, $\beta = 90.4°$, $\gamma = 120.6°$). We present an energy−volume curve in Figure S2 that shows the results of this procedure for our loaded SSZ-13 unit cell. Additionally, we attach a crystallographic information file of the optimized loaded SSZ-13 unit cell as Supporting Information.

https://dx.doi.org/10.1021/acscatal.0c01590
ACS Catal. 2020, 10, 9410−9419

3. RESULTS AND DISCUSSION

3.1. Repositioning of Cu Ions in Hydrothermal Aging.

Figure 3 displays H_2-TPR profiles for the fresh and HTA

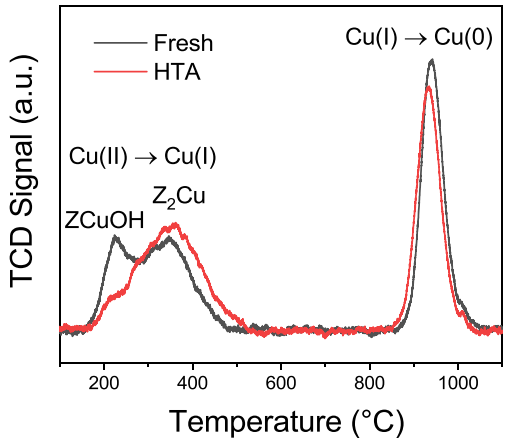

Figure 3. H_2-TPR results for the fresh and HTA Cu/SSZ-13 catalyst.

samples. The fresh sample displays two low-temperature reduction peaks: one centered at ~220 °C that can be assigned to the reduction of ZCuOH to ZCu(I) and another centered at ~350 °C that is attributed to the reduction of Z_2Cu to ZCu(I).[14,22,38] The high-temperature reduction peak centered at ~950 °C is attributed to the reduction of ZCu(I) to Cu(0).[30] The essentially identical peak areas of the low- and high-temperature reduction states indicate the absence of CuO_x clusters in this catalyst; CuO_x clusters can only contribute to the low-temperature state since these are readily reduced to Cu(0) around 300 °C.[23,39,40] For the HTA sample, the ~220 °C reduction peak greatly diminishes, accompanied by an apparent intensity increase of the ~350 °C peak. This is caused by the conversion of ZCuOH to Z_2Cu during aging (i.e., ZCuOH + ZH → Z_2Cu + H_2O).[21] The high-temperature reduction peak for this sample shifts very slightly to lower temperatures as compared to the fresh sample. It is important to note that both low- and high-temperature peak areas of the HTA sample resemble those of the fresh catalyst, suggesting the essential absence of Cu-ion agglomeration to CuO_x during aging. This is consistent with the fact that the hydrothermal aging temperature of 600 °C applied here will not cause any dealumination of the Cu/SSZ-13 catalyst.[21] Therefore, the rather mild hydrothermal aging treatment here only causes location changes for certain isolated Cu(II) ions but imposes no influence on the structural integrity of the SSZ-13 support. This conclusion is also strongly supported by similar ZCu(I) to Cu(0) reduction temperatures of the two samples. This follows since this high-temperature reduction stage coincides with the collapse of the chabazite structure; similar reduction temperatures suggest similar structural integrity of the supports. It has been demonstrated previously that for Cu/SSZ-13 catalysts with obvious framework degradation, ZCu(I) reduction occurs at much lower temperatures.[23,39] Using Ag_2O reduction as the reference, the Cu content in both samples is estimated to be ~1.4 wt %, which is very close to the ICP result shown above. In principle, Z_2Cu and ZCuOH contents in both samples can be readily estimated by peak fitting of the low-temperature reduction states. However, since our TPR measurements were carried out on fully hydrated samples (to avoid ZCuOH autoreduction in a dehydration pretreatment), ZCuOH contents can be substantially overestimated: as shown by Martini et al., rather high percentages of Cu can be kinetically stabilized as ZCuOH in low Si/AlCu/SSZ-13 samples prior to full dehydration.[41] More accurate quantification of Z_2Cu and ZCuOH with EPR will be given below.

Figure 4a shows the EPR spectra for hydrated fresh and HTA samples measured at ambient temperature, where sample

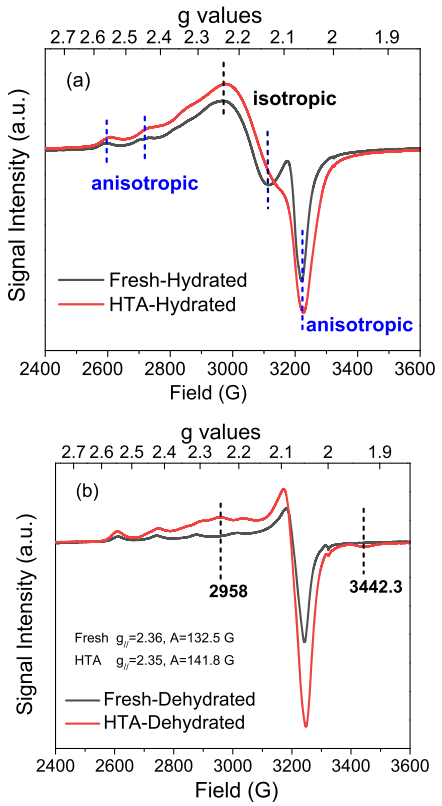

Figure 4. (a) EPR spectra for hydrated fresh and HTA samples measured at room temperature. (b) EPR spectra for dehydrated fresh and HTA samples measured at 50 °C.

hydration was achieved by exposing the samples to the open laboratory air for extended periods. In this case, all isolated Cu^{2+} species are anticipated to be EPR-active.[27,30] As shown in the figure, both samples display a feature at ~3100 G in the high field, which is assigned to isotropic Cu(II) ions, i.e., fully hydrated Z_2Cu and ZCuOH as $[Cu(H_2O)_6]^{2+}$ and $[Cu(H_2O)_5OH]^{+}$ species, respectively.[42] These species are mobile inside the CHA cages and display minimal interactions with the zeolite framework. As such, they do not display hyperfine features but rather a partially averaged spectrum. Both samples also display a stronger feature at ~3220 G in the high field, which is assigned to immobilized Cu(II) ions, i.e., partially hydrated Z_2Cu and ZCuOH as $[Cu(O_L)_x(H_2O)_{6-x}]^{2+}$ and $[Cu(O_L)_x(H_2O)_{5-x}OH]^{+}$ species (O_L represents zeolite lattice oxygen). Such species are much less mobile and therefore do show hyperfine features associated with a typical axial copper spectrum. Note that if the mobile hydrated Cu(II) ions are "immobilized" by cooling the samples to cryogenic temperatures, then these two types of Cu(II) ions become EPR-indistinguishable, as is clearly shown in Figure 2a. A comparison between the fresh and HTA samples reveals that aging treatment causes an increase of anisotropic Cu(II) content; i.e., some loosely bound Cu(II) species convert to strongly bound Cu(II)

https://dx.doi.org/10.1021/acscatal.0c01590
ACS Catal. 2020, 10, 9410−9419

during aging. This is in line with the H_2-TPR data showing ZCuOH conversion to Z_2Cu during hydrothermal aging (Figure 3). Via quantitation of the EPR-active copper by double integration of the EPR spectra, it is found that both samples contain essentially the same amounts of EPR-active Cu(II); this again confirms the absence of CuO_x clusters in the HTA sample.

Figure 4b presents EPR spectra for dehydrated fresh and HTA samples measured at 50 °C, where dehydration was achieved by flowing dry N_2 through the EPR tube containing the hydrated sample held at 250 °C until spectral lineshapes became invariant with time. After dehydration, all EPR-active Cu(II) sites become anisotropic with well-resolved hyperfine signals. For the fresh sample, the spin Hamiltonian parameters of $g_{\|}$ = 2.36 and A = 132.5 G suggest that the majority of isolated Cu(II) ions are located in windows of 6MR binding to three O_L.[25] For the HTA sample, the corresponding tensor values become $g_{\|}$ = 2.35 and A = 141.8 G. According to previous studies, decreased $g_{\|}$ and increased A values suggest an increase in charge delocalization for Cu−O coordination systems.[43,44] This indicates that EPR-active Cu(II) ions in the HTA sample become less positively charged on average than those of the fresh sample, again consistent with the increased Cu−zeolite interactions for the former. By double integration of the EPR spectra of the dehydrated samples and by comparison to their hydrated counterparts, ∼78% of Cu in the dehydrated fresh sample remains EPR-active, whereas for the dehydrated HTA sample, ∼90% remains EPR-active. Since EPR-active, hydrated ZCuOH only converts to EPR-silent species during dehydration (i.e., dehydrated ZCuOH, autoreduced ZCu(I), and dimeric Cu−O−Cu moieties),[18] such EPR quantifications suggest that the fresh sample contains ∼22% ZCuOH and the HTA sample contains ∼10% ZCuOH, i.e., ∼12% of Cu converts from ZCuOH to Z_2Cu during hydrothermal aging.

Interestingly, the dehydrated HTA sample studied here again shows a positive EPR peak at 2958 G and a negative peak at 3442 G (Figure 4b), the same as the dehydrated HTA samples shown in Figure 2b. These unusual features are due to interspin interactions between pairs of isolated EPR-active Cu centers. The fact that they are not present in dehydrated fresh samples or any hydrated samples suggests that the Cu−Cu distance plays a decisive role for their appearance; only paired isolated Cu(II) sites spatially positioned within a relatively short distance give rise to these unusual split EPR signals. It is known from the literature that the distance between two unpaired electrons from EPR powder spectra can be estimated using a simplified equation as follows[45]

$$D = \frac{3g\beta}{2r^3} = 1.39 \times 10^4 \frac{g}{r^3} \quad (1)$$

where D is the splitting between the two peaks in gauss, $g_{\perp}$ = 2.07 for unpaired electrons, and r is the distance between the two unpaired electrons in Ångstroms. Using Figure 4b, D is measured as D = 3442 G − 2958 G = 484 G. This allows r to be readily estimated to be 3.90 Å. This calculation makes several assumptions: first, the energy difference between the two coppers is smaller than the dipolar energy. Although the overall width of the copper spectrum is larger than the dipolar splitting, the peaks being analyzed are symmetric about the $g_{\perp}$ region and the bulk of the spectral density is well within this splitting. It is also assumed that there is little exchange coupling; however, these coppers share no bridging ligands making the likelihood of an orbital overlap rather small.[46] This calculation also does not consider the angle between the two coppers and the z-axis of the individual copper spin system. If all (i.e., a random distribution such as in a solution) orientations are not allowed, then the dipolar spectrum will not be the classic Pake pattern. However, this dipolar spectrum will have the same limits and turning points, and it will just have intensities redistributed.

In the following, DFT calculations were applied to answer (1) what exchange positions allow two isolated Cu(II) cations to have a physical separation of ∼3.90 Å and (2) why these paired structures are not present in dehydrated fresh catalysts. Our calculations demonstrate that such a structure with such a short distance is only possible when placing two Cu(II) ions in the two windows of a double 6MR prism. Note that by placing two Cu(II) ions into the same chabazite cage, each occupying a 8MR window position will not result in a structure with the Cu cations that are ∼3.90 Å apart because of the large dimensions of the zeolite cage. We tested all possible arrangements with two Al atoms in one 6MR and two in the other 6MR of the prism. When considering Löwenstein's rule, this results in five distinct relative positions, which are shown in Figure S3. In the most energetically favorable of our tested double Z_2Cu configurations in the double 6MR windows, we find the Cu−Cu bond distance to be 3.97 Å, which agrees quite well with the EPR measurements. We note that the Cu−Cu distances of the less energetically favorable (by at most 0.11 eV) structures are similar to those of the most energetically favorable structure. These additional data points help support the claim that the Cu−Cu distance of two Cu(II) ions positioned in a double 6MR prism is around the experimentally observed value invariant of specific Al positioning. This supports the experimental claim that EPR data estimates for this distance originate from pairs of Cu(II) ions in the double 6MR prism without relying on specific Al positioning within the prism. Therefore, the original structure model by Fickel and Lobo (Figure 1) correctly described this structure.

Additionally, theoretical calculations were used to support the idea that double Z_2Cu configurations in the double 6MR prism do not exist in freshly prepared catalysts. In a fresh catalyst, the experimental results (Figures 2b, 4b) show that if one window of the double 6MR prism is occupied by a Cu(II) cation, the other window will be unoccupied. In response to this, we modeled the ZCuOH + ZH → Z_2Cu + H_2O reaction, where Z_2Cu is in one window of the double 6MR prism and ZCuOH is in a nearby 8MR, to a double Z_2Cu configuration in the double 6MR prism (Figure 5, see Figure S4 in the Supporting Information for a slightly less energetically favorable alterative). In our calculations, we find this process to be mildly endothermic (∼0.2 eV). Due to the relatively small magnitude of the reaction energy, this is certainly a feasible reaction under hydrothermal treatment

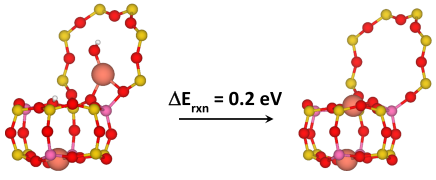

Figure 5. Schematic of the ZCuOH + ZH → Z_2Cu + H_2O reaction that leads to the formation of the structure that gives rise to the unusual EPR signals highlighted in Figures 2b and 4b. During this reaction, the Cu-Cu bond distance changes from 7.00 Å to 3.97 Å. The white spheres are hydrogen atoms while the sphere legend for the other atoms are as in Figure 1. We note that the formed water molecule is not displayed since it is assumed to be infinitely separated from the Cu cations.

https://dx.doi.org/10.1021/acscatal.0c01590
ACS Catal. 2020, 10, 9410−9419

conditions. Thus, it is unsurprising that this configuration is observed after such a treatment. However, it is still puzzling why the same configuration is not observed in the fresh catalyst, considering that it was calcined in air at 550 °C after Cu-exchange, where small activation barriers should be readily overcome. It is likely that the activation barrier for the generation of the double Z_2Cu configuration is rather high under the "dry" condition, and the presence of high concentrations of water vapor (a situation met under hydrothermal aging) is essential to lower that. Note particularly that there has been rich literature demonstrating that proton transport in zeolite pores is greatly facilitated by water,[47,48] which can certainly promote the $ZCuOH + ZH \rightarrow Z_2Cu + H_2O$ reaction by bringing protons close to the ZCuOH conformation. We are currently modeling this from a computational perspective (i.e., increasing the water density in the pores); the results will be reported elsewhere. It is important to note, however, that even in hydrothermally aged catalysts, the double Z_2Cu configurations in the double 6MR prism are rather minor, estimated to be only a few percent of all Cu based on the weak EPR signals that such paired species generate.

3.2. SCR Performance Loss Due to Repositioning of Cu Ions. So far, we have shown that under our rather mild hydrothermal aging conditions, the chabazite structure of the SSZ-13 support does not degrade and isolated Cu(II) ions do not agglomerate. However, considerable isolated Cu(II)-ion relocation occurs; the appearance of EPR signals due to coupling of Cu ions ~3.9 Å apart provides good evidence for at least a portion of such relocation. As shown in Figure 4a, a considerable decrease in the amount of isotropic Cu(II) ions is found in the hydrated HTA sample. This suggests that hydrothermal aging also induces stronger Cu−zeolite interactions even to Cu sites that do not form the double Z_2Cu configurations in the double 6MR prism. In addition to the $ZCuOH + ZH \rightarrow Z_2Cu + H_2O$ reaction that occurs to ~10% of total Cu(II) species as determined with EPR quantification, it is also possible that some Cu(II) ions only reposition slightly (e.g., by adjusting Cu−O distances) during aging. Next, this notion was further demonstrated via NH_3 chemisorption probed by EPR.

NH_3, which solvates Cu ions more readily than H_2O, was used to further probe differences between our fresh and HTA samples. In this case, 500 ppm NH_3/N_2 was introduced to dehydrated fresh and HTA samples at 50 °C, during which EPR spectra were continuously recorded until the spectral lineshapes no longer changed with time (i.e., saturation). The time-dependent EPR spectra are shown in Figure S5; the EPR spectra upon NH_3 saturation are presented in Figure 6. For the fresh catalyst, a broad high-field feature is found at ~3300 G, which differs considerably from the sharper ~3250 G signal attributed to dehydrated Z_2Cu shown in Figure 4b. The signal broadness suggests a distribution of the closely related structure yielding the superposition of multiple EPR spectra. Meanwhile, the hyperfine-region EPR parameters become $g_{\|} = 2.26$ and $A = 174$ G, also differing considerably from $g_{\|} = 2.36$ and $A = 132.5$ G attributed to dehydrated Z_2Cu. Such changes are readily attributed to the formation of EPR-active Cu(II)−NH_3 complexes.[26,49,50] It is also shown in Figure 6 that the high-field signal at 3442 G for the HTA sample, attributed to double Z_2Cu in double 6MR, completely disappears upon NH_3 saturation. This is readily understood: as with H_2O ligands, NH_3 "pulls" Cu(II) ions from the 6MR windows toward the chabazite cages, thus diminishing coupling between the two formerly nearby Cu(II) ions.[45]

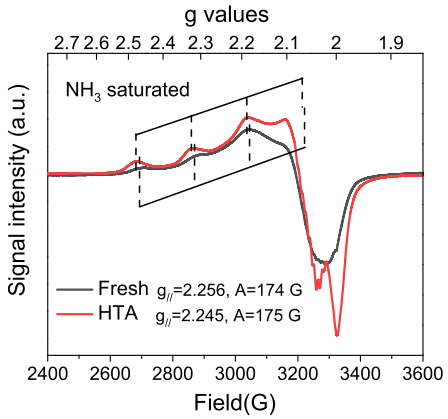

Figure 6. EPR spectra for NH_3-saturated fresh and HTA Cu/SSZ-13 samples at 50 °C.

Note also that the NH_3-saturated HTA sample displays two high-field peaks centered at ~3180 and ~3340 G with EPR parameters $g_{\|} = 2.25$ and $A = 175$ G. The presence of the doubled high-field features may suggest spectroscopic distinction between Cu(II)−NH_3 complexes with different mobility, e.g., more mobile $[Cu(NH_3)_4]^{2+}$ and $[Cu(NH_3)_3OH]^{+}$ species versus less mobile $[Cu(O_L)_x(NH_3)_{4-x}]^{2+}$ and $[Cu(O_L)_x(NH_3)_{3-x}OH]^{+}$,[13,21] analogous to hydrated samples shown in Figure 4a. However, our Easyspin simulations[51] suggest that the formation of the two high-field peaks here is not due to multiple species but to the large A value causing the highest-field hyperfine line to overlap the $g_{\perp}$ region. Therefore, the spectrum lineshape difference between NH_3-saturated fresh and HTA samples is better interpreted as that the HTA sample contains Cu ions with better uniformity of structure (i.e., more structurally identical Z_2Cu sites) than the fresh catalyst. It is clear, again, that the Cu(II)−NH_3 complexes in the fresh catalyst receive less framework restriction than those in the HTA catalyst: high-field superhyperfine structures (i.e., "spikes" on the high-field signals) from ^{14}N for the fresh catalyst are almost indistinguishable, whereas in the HTA spectra, such signals are clearly better resolved due to mobility restrictions of the Cu−NH_3 complexes. In the following, we demonstrate how the SCR performance is influenced by the Cu location differences between fresh and HTA catalysts by applying SCR kinetics and in situ EPR studies.

Figure 7a presents steady-state standard SCR ($4NO + 4NH_3 + O_2 \rightarrow 4\ N_2 + 6H_2O$) light-off curves for the two catalysts. Below 350 °C, the fresh catalyst outperforms the HTA sample as a result of decreased turnover rates for the latter catalyst. Above this temperature, however, no obvious performance difference is observed. The similarity in high temperature selectivities for both catalysts is fully in line with the absence of CuO_x formation during hydrothermal aging. To gain useful kinetic information from the low NO_x conversion data points (differential conversions), reaction rates were normalized using the first-order kinetic equation, i.e., $r = \frac{F}{w}(-\ln(1 - x))$, where F is the NO_x flow rate (moles of NO_x per second), w is the mass of the catalyst (g), and x is the NO_x conversion. The normalized rate versus temperature plots are shown in Figure S6 of the Supporting Information. As shown in Figure 7b, Arrhenius plots using normalized rate data at differential conversions demonstrate that under kinetic control, turnover rates over the fresh catalyst are ~2 times those of the HTA sample measured under the same conditions. Such a performance loss for the

https://dx.doi.org/10.1021/acscatal.0c01590
ACS Catal. 2020, 10, 9410−9419

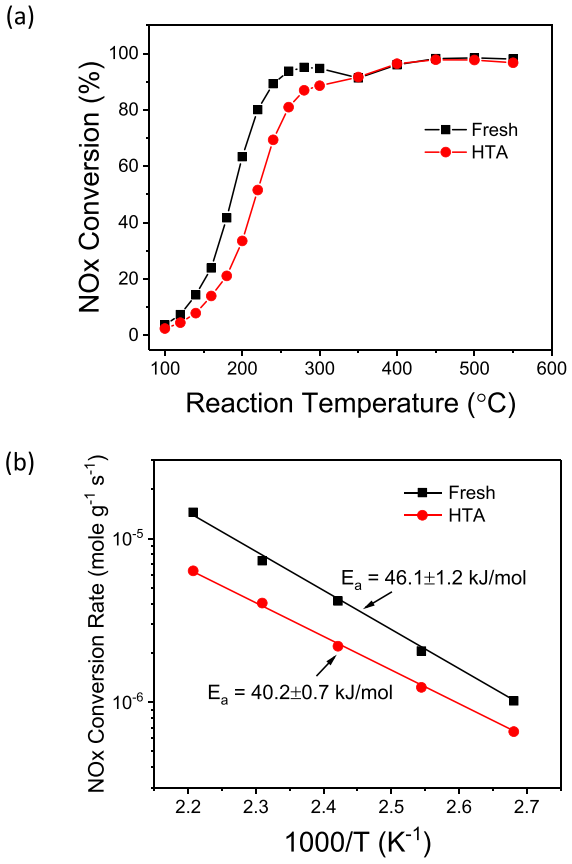

Figure 7. (a) The NOx conversion versus temperature plots (light-off curves) for steady-state standard SCR over fresh and HTA Cu/SSZ-13 catalysts. The reactant feed was as follows: 360 ppm NO, 360 ppm NH_3, 10% O_2 balanced with N_2. 90 mg of catalysts were used, total gas flow was 900 mL/min, corresponding to a GHSV of 400,000 h^{-1}. (b) The corresponding Arrhenius plots generated using normalized SCR rates (mole NOx per $g_{cat.}$ Per second) within the kinetics-controlled regime. Apparent activation energies are marked adjacent to the plots.

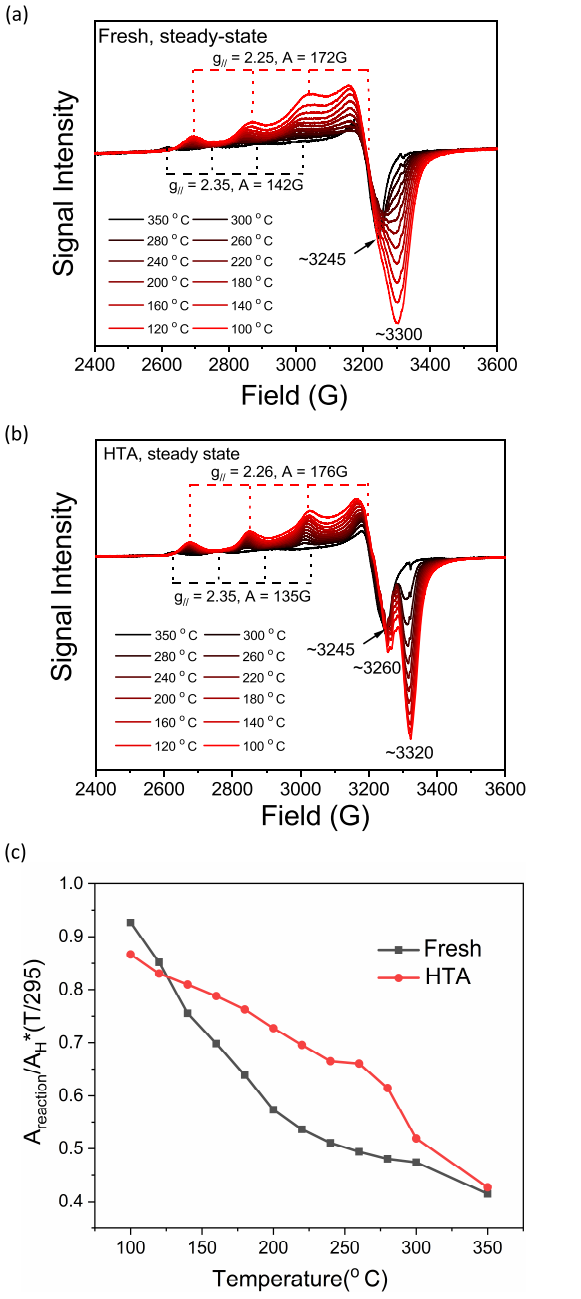

Figure 8. (a) EPR spectra acquired at selected temperatures during standard NH_3-SCR over the fresh Cu/SSZ-13 catalyst. (b) EPR spectra acquired over the HTA catalyst. (c) Ratios between EPR active Cu and total Cu as a function of reaction temperature. Reactant composition 360 ppm NO, 360 ppm NH_3, 10% O_2 balanced with N_2. 10 mg of catalysts were used in the tests, total gas flow was 100 mL/min, corresponding to a GHSV of 400,000 h^{-1}.

HTA sample is remarkable considering that the amount of SCR active Cu and the integrity of the SSZ-13 support do not change appreciably during hydrothermal aging. Note also that the fresh catalyst displays an apparent activation energy that is ~6 kJ/mol higher than that of the HTA sample. Such a small difference suggests the same SCR mechanism for the two catalysts.

To rationalize the performance difference of the two catalysts, in situ EPR measurements were carried out at the same reactant composition and space velocity as those shown above. At each tested reaction temperature, between 100 and 350 °C, an EPR spectrum was collected upon arrival of a steady state. Spectra acquired over the fresh catalyst are depicted in Figure 8a. As the temperature rises from 100 to 350 °C, the high-field signals shift gradually from ~3300 to ~3245 G and the hyperfine region tensor values also change from $g_{||}$ = 2.25 and A = 172 G to $g_{||}$ = 2.35 and A = 142 G. As compared to the EPR parameters of the dehydrated and NH_3-saturated samples, it can be concluded that EPR-visible Cu(II) gradually converts from Cu(II)−NH_3 complexes to Cu(II)−O_L complexes. From the data shown in Figure 8b, the HTA sample displays the same trend as a function of temperature. However, at all temperatures tested here, these two catalysts show the same difference under reaction conditions as that shown in Figure 6 during NH_3 chemisorption: Cu(II)−NH_3 complexes in the HTA sample display stronger framework restrictions than those in the fresh catalyst as evidenced by the clear distinction of different high-field signals.

Due to the quantitative nature of EPR, EPR-active Cu(II) species under reaction conditions were quantified by signal double integration and ratioed against the total Cu content, obtained by double integrating the hydrated sample signal (A_{SCR}/A_{total}); the results are depicted in Figure 8c. Note that the EPR signal intensity is inversely proportional to temperature (in kelvin); such ratios were normalized accordingly. From the plots, it is seen that from the temperature where light-off initiates (~125 °C) to 350 °C, the HTA catalyst contains higher

https://dx.doi.org/10.1021/acscatal.0c01590
ACS Catal. 2020, 10, 9410−9419

percentages of EPR-active Cu(II) than the fresh catalyst. Recent studies documented clearly that standard SCR follows a redox mechanism, comprising a reduction half-cycle, Cu(II) → Cu(I), where Cu(II) sites are reduced to Cu(I) by NO + NH_3, and an oxidation half-cycle, Cu(I) → Cu(II), where Cu(I) species are oxidized back to Cu(II) by NO + O_2, to close the redox cycling.[16,17,52] It is anticipated that highly stable Cu(II) and Cu(I) intermediates slow down the SCR reaction by maintaining the same oxidation state. Indeed, Zhang et al.[53] have demonstrated recently that Cu(II)−NH_3 complexes with different NH_3 ligand numbers display different reactivities.

It has been proposed that the most stable intermediate under low-temperature (≤250 °C) standard SCR reaction conditions is a linear $[Cu(I)(NH_3)_2]^+$ intermediate.[3,13,16,17] Since O_2 activation requires the participation of two such intermediates, the Cu(I) → Cu(II) reactions become rate-limiting for low-Cu loaded catalysts.[16,17] However, Cu(I) → Cu(II) does not appear to be rate-limiting here since the less active HTA catalyst contains lower concentrations of Cu(I) during our low-temperature SCR tests. Therefore, we propose here that under mild hydrothermal aging conditions (i.e., without loss of isolated Cu(II) sites and zeolite support structure degradation), the mechanism for activity loss is relocation of isolated Cu(II) ions such that they are stabilized relative to their pretreatment state.

Fully NH_3-solvated Cu(II) sites, i.e., $[Cu(II)(NH_3)_4]^{2+}$ and $[Cu(II)(OH)(NH_3)_3]^+$, have recently been proposed as low-temperature SCR active species.[13,54] For such symmetrical species to activate NO in order to form the proposed $[Cu(I)(NH_3)_2]^+$−H_2NNO transition state,[13] elongation of one Cu(II)−NH_3 bond is required so that the NO molecule can effectively coordinate to the Cu center. Based on DFT calculations, all four NH_3 ligands in the $[Cu(II)(NH_3)_4]^{2+}$ complex display similar adsorption energies of ∼130 kJ/mol with the Cu center. Similarly, all three NH_3 ligands in the $[Cu(II)\ (OH)(NH_3)_3]^+$ complex display similar adsorption energies of ∼120 kJ/mol with the Cu center.[13] Therefore, for fully NH_3-solvated Cu(II) moieties, Cu(II)−NH_3 bond elongation should happen to all NH_3 ligands with equal possibilities. For partially NH_3-solvated Cu(II) sites that our in situ EPR data suggest to be present in the HTA sample, e.g., $[Cu(II)(O_L)_2(NH_3)_2)]^{2+}$, two likely reasons can be considered for their lower activity as compared to their fully NH_3-solvated counterparts. First, the framework O_L ligands may impose electronic effects rendering stronger Cu(II)−NH_3 bonding and therefore less reactive Cu(II) center. Second, framework shielding (i.e., Cu−O_L bonding) renders the Cu(II) center only partly accessible to NO. From our current results, no further insights can be made. More work is needed to further elucidate the underlying causes for the decreased rates for the HTA sample.

4. CONCLUSIONS

The present study was initiated by searching for isolated Cu(II) sites within SSZ-13 that display exceedingly small EPR interspin distances of ∼3.9 Å. With the aid of DFT calculations, such Cu sites are identified as a paired Cu(II) species, each staying in one 6MR window of a double 6MR prism, which form exclusively under hydrothermal aging conditions. However, such Cu species only account for a small percentage of Cu in the catalyst and thus cannot explain the 2-fold SCR rate loss of the catalyst after mild hydrothermal aging. Additional EPR comparisons between fresh and aged catalysts in their hydrated, dehydrated, and NH_3-saturated forms reveal that the Cu(II) species in the aged catalyst displays higher degrees of immobility as a result of stronger Cu−zeolite support interactions. Accompanying in situ EPR measurements under steady-state SCR conditions show evidence of such stronger Cu−support interactions that render Cu(II) intermediates less reactive, thus slowing down SCR turnover rates.

■ ASSOCIATED CONTENT

Supporting Information

The Supporting Information is available free of charge at https://pubs.acs.org/doi/10.1021/acscatal.0c01590.

(S1): Schematic structures for (a) Z_2Cu structure A, (b) Z_2Cu structure B, and (c) ZCuOH. (S2): Energy versus volume curve for the unit cell optimization of the hexagonal Cu-SSZ-13 unit cell. (S3): The Cu−Cu bond distances and relative DFT energies of the tested SSZ-13 hexagonal unit cell. (S4): Slightly less favorable reaction pathway for ZCuOH + ZH → Z_2Cu + H_2O. (S5): Series of EPR spectra recorded during exposure of 100 mL/min 500 ppm NH_3/N_2 at 323 K to (a) fresh and (b) HTA Cu/SSZ-13 samples. (S6): Normalized NO_x conversion rate versus temperature plots for steady-state standard SCR over fresh and HTA Cu/SSZ-13 catalysts (PDF)

Crystallographic data for the DFT-based structures (CIF)

■ AUTHOR INFORMATION

Corresponding Authors

Junhua Li − *State Key Joint Laboratory of Environment Simulation and Pollution Control, School of Environment, Tsinghua University, Beijing 100084, China;* orcid.org/0000-0001-7249-0529; Email: lijunhua@tsinghua.edu.cn

Eric D. Walter − *Environmental Molecular Sciences Laboratory, Pacific Northwest National Laboratory, Richland, Washington 99354, United States;* orcid.org/0000-0003-3644-5514; Email: eric.walter@pnnl.gov

Feng Gao − *Institute for Integrated Catalysis, Pacific Northwest National Laboratory, Richland, Washington 99354, United States;* orcid.org/0000-0002-8450-3419; Email: feng.gao@pnnl.gov

Authors

Yani Zhang − *State Key Joint Laboratory of Environment Simulation and Pollution Control, School of Environment, Tsinghua University, Beijing 100084, China; Institute for Integrated Catalysis, Pacific Northwest National Laboratory, Richland, Washington 99354, United States*

Yue Peng − *State Key Joint Laboratory of Environment Simulation and Pollution Control, School of Environment, Tsinghua University, Beijing 100084, China;* orcid.org/0000-0001-5772-3443

Kyle Groden − *The Gene and Linda Voiland School of Chemical Engineering and Bioengineering, Washington State University, Pullman, Washington 99164, United States*

Jean-Sabin McEwen − *Institute for Integrated Catalysis, Pacific Northwest National Laboratory, Richland, Washington 99354, United States; The Gene and Linda Voiland School of Chemical Engineering and Bioengineering, Department of Physics and Astronomy, Department of Chemistry, and Department of Biological Systems Engineering, Washington State University, Pullman, Washington 99164, United States;* orcid.org/0000-0003-0931-4869

https://dx.doi.org/10.1021/acscatal.0c01590
ACS Catal. 2020, 10, 9410−9419

Ying Chen − *Environmental Molecular Sciences Laboratory, Pacific Northwest National Laboratory, Richland, Washington 99354, United States;* orcid.org/0000-0001-7417-0991

Yong Wang − *Institute for Integrated Catalysis, Pacific Northwest National Laboratory, Richland, Washington 99354, United States; The Gene and Linda Voiland School of Chemical Engineering and Bioengineering, Washington State University, Pullman, Washington 99164, United States;* orcid.org/0000-0002-8460-7410

Complete contact information is available at: https://pubs.acs.org/10.1021/acscatal.0c01590

Notes

The authors declare no competing financial interest.

■ ACKNOWLEDGMENTS

The authors from Pacific Northwest National Laboratory (PNNL) gratefully acknowledge the U.S. Department of Energy (DOE), Energy Efficiency and Renewable Energy, Vehicle Technologies Office for the support of this work. The research described in this paper, including DFT calculations, was performed in the Environmental Molecular Sciences Laboratory (EMSL), a national scientific user facility sponsored by the DOE's Office of Biological and Environmental Research and located at PNNL. PNNL is operated for the U.S. DOE by Battelle. The authors from Tsinghua University acknowledge the Joint-Training Scholarship provided by the China Scholarship Council (CSC) for Y.Z.'s visit to PNNL. Financial support to WSU was provided by the National Science Foundation CAREER program under contract No. CBET-1653561. J.-S.M. thanks Samantha Bennett for fruitful discussions. The authors are grateful to Dr. Charles H.F. (Chuck) Peden (PNNL) for his insightful comments and careful editing of the manuscript.

■ REFERENCES

(1) Gao, F.; Kwak, J. H.; Szanyi, J.; Peden, C. H. F. Current Understanding of Cu-exchanged Chabazite Molecular Sieves for Use as Commercial Diesel Engine DeNOx Catalysts. *Top. Catal.* **2013**, *56*, 1441−1459.

(2) Beale, A. M.; Gao, F.; Lezcano-Gonzalez, I.; Peden, C. H. F.; Szanyi, J. Recent Advances in Automotive Catalysis for NOx Emission Control by Small-pore Microporous Materials. *Chem. Soc. Rev.* **2015**, *44*, 7371−7405.

(3) Gao, F.; Peden, C. H. F. Recent Progress in Atomic-level Understanding of Cu/SSZ-13 Selective Catalytic Reduction Catalysts. *Catalysts* **2018**, *8*, 140.

(4) Paolucci, C.; Di Iorio, J. R.; Ribeiro, F. H.; Gounder, R.; Schneider, W. F. Catalysis Science of NO_x Selective Catalytic Reduction with Ammonia over Cu-SSZ-13 and Cu-SAPO-34. *Adv. Catal.* **2016**, *59*, 1−107.

(5) Borfecchia, E.; Beato, P.; Svelle, S.; Olsbye, U.; Lamberti, C.; Bordiga, S. Cu-CHA - a Model System for Applied Selective Redox Catalysis. *Chem. Soc. Rev.* **2018**, *47*, 8097−8133.

(6) Fickel, D. W.; Lobo, R. F. Copper Coordination in Cu-SSZ-13 and Cu-SSZ-16 Investigated by Variable-temperature XRD. *J. Phys. Chem. C* **2010**, *114*, 1633−1640.

(7) Korhonen, S. T.; Fickel, D. W.; Lobo, R. F.; Weckhuysen, B. M.; Beale, A. M. Isolated Cu^{2+} Ions: Active Sites for Selective Catalytic Reduction of NO. *Chem. Commun.* **2011**, *47*, 800−802.

(8) Kwak, J. H.; Zhu, H.; Lee, J. H.; Peden, C. H. F.; Szanyi, J. Two Different Cationic Positions in Cu-SSZ-13? *Chem. Commun.* **2012**, *48*, 4758−4760.

(9) Giordanino, F.; Vennestrøm, P. N. R.; Lundegaard, L. F.; Stappen, F. N.; Mossin, S.; Beato, P.; Bordiga, S.; Lamberti, C. Characterization of Cu-exchanged SSZ-13: a Comparative FTIR, UV-Vis, and EPR Study with Cu-ZSM-5 and Cu-beta with Similar Si/Al and Cu/Al Ratios. *Dalton Trans.* **2013**, *42*, 12741−12761.

(10) Kim, Y. J.; Lee, J. K.; Min, K. M.; Hong, S. B.; Nam, I. S.; Cho, B. K. Hydrothermal Stability of Cu-SSZ13 for Reducing NO_x by NH_3. *J. Catal.* **2014**, *311*, 447−457.

(11) Andersen, C. W.; Bremholm, M.; Vennestrøm, P. N. R.; Blichfeld, A. B.; Lundegaard, L. F.; Iversen, B. B. Location of Cu^{2+} in CHA Zeolite Investigated by X-ray Diffraction Using the Rietveld/Maximum Entropy Method. *IUCrJ* **2014**, *1*, 382−386.

(12) Borfecchia, E.; Lomachenko, K. A.; Giordanino, F.; Falsig, H.; Beato, P.; Soldatov, A. V.; Bordiga, S.; Lamberti, C. Revisiting the Nature of Cu Sites in the Activated Cu-SSZ-13 Catalyst for SCR Reaction. *Chem. Sci.* **2015**, *6*, 548−563.

(13) Paolucci, C.; Parekh, A. A.; Khurana, I.; Di Iorio, J. R.; Li, H.; Caballero, J. D. A.; Shih, A. J.; Anggara, T.; Delgass, W. N.; Miller, J. T.; Ribeiro, F. H.; Gounder, R.; Schneider, W. F. Catalysis in a Cage: Condition-dependent Speciation and Dynamics of Exchanged Cu Cations in SSZ-13 Zeolites. *J. Am. Chem. Soc.* **2016**, *138*, 6028−6048.

(14) Gao, F.; Washton, N. M.; Wang, Y.; Kollár, M.; Szanyi, J.; Peden, C. H. F. Effects of Si/Al Ratio on Cu/SSZ-13 NH_3-SCR Catalysts: Implications for the Active Cu Species and the Roles of Brønsted Acidity. *J. Catal.* **2015**, *331*, 25−38.

(15) Göltl, F.; Bulo, R. E.; Hafner, J.; Sautet, P. What Makes Copper-exchanged SSZ-13 Zeolite Efficient at Cleaning Car Exhaust Gases? *J. Phys. Chem. Lett.* **2013**, *4*, 2244−2249.

(16) Gao, F.; Mei, D.; Wang, Y.; Szanyi, J.; Peden, C. H. F. Selective Catalytic Reduction over Cu/SSZ-13: Linking Homo- and Heterogeneous Catalysis. *J. Am. Chem. Soc.* **2017**, *139*, 4935−4942.

(17) Paolucci, C.; Khurana, I.; Parekh, A. A.; Li, S.; Shih, A. J.; Li, H.; Di Iorio, J. R.; Albarracin-Caballero, J. D.; Yezerets, A.; Miller, J. T.; Delgass, W. N.; Ribeiro, F. H.; Schneider, W. F.; Gounder, R. Dynamic Multinuclear Sites Formed by Mobilized Copper Ions in NO_x Selective Catalytic Reduction. *Science* **2017**, *357*, 898−903.

(18) Song, J.; Wang, Y.; Walter, E. D.; Washton, N. M.; Mei, D.; Kovarik, L.; Engelhard, M. H.; Prodinger, S.; Wang, Y.; Peden, C. H. F.; Gao, F. Toward Rational Design of Cu/SSZ-13 Selective Catalytic Reduction Catalysts: Implications from Atomic-level Understanding of Hydrothermal Stability. *ACS Catal.* **2017**, *7*, 8214−8227.

(19) Gao, F.; Szanyi, J. On the Hydrothermal Stability of Cu/SSZ-13 SCR Catalysts. *Appl. Catal., A* **2018**, *560*, 185−194.

(20) Luo, J.; Wang, D.; Kumar, A.; Li, J.; Kamasamudram, K.; Currier, N.; Yezerets, A. Identification of Two Types of Cu Sites in Cu/SSZ-13 and Their Unique Responses to Hydrothermal Aging and Sulfur Poisoning. *Catal. Today* **2016**, *267*, 3−9.

(21) Luo, J.; Gao, F.; Kamasamudram, K.; Currier, N.; Peden, C. H. F.; Yezerets, A. New Insights into Cu/SSZ-13 SCR Catalyst Acidity. Part I: Nature of Acidic Sites Probed by NH_3 Titration. *J. Catal.* **2017**, *348*, 291−299.

(22) Gao, F.; Wang, Y.; Washton, N. M.; Kollar, M.; Szanyi, J.; Peden, C. H. F. Effects of Alkali and Alkaline Earth Cocations on the Activity and Hydrothermal Stability of Cu/SSZ-13 NH_3-SCR Catalysts. *ACS Catal.* **2015**, *5*, 6780−6791.

(23) Cui, Y.; Wang, Y.; Walter, E. D.; Szanyi, J.; Wang, Y.; Gao, F. Influences of Na^+ Co-cation on the Structure and Performance of Cu/SSZ-13 Selective Catalytic Reduction Catalysts. *Catal. Today* **2020**, *339*, 233−240.

(24) Villamaina, R.; Liu, S.; Nova, I.; Tronconi, E.; Ruggeri, M. P.; Collier, J.; York, A.; Thompsett, D. Speciation of Cu Cations in Cu-CHA Catalysts for NH_3-SCR: Effects of SiO_2/AlO_3 Ratio and Cu-loading Investigated by Transient Response Methods. *ACS Catal.* **2019**, *9*, 8916−8927.

(25) Fernández, E.; Moreno-González, M.; Moliner, M.; Blasco, T.; Boronat, M.; Corma, A. Modeling of EPR Parameters for Cu(II): Application to the Selective Reduction of NO_x Catalyzed by Cu-zeolites. *Top. Catal.* **2018**, *61*, 810−832.

(26) Moreno-González, M.; Hueso, B.; Boronat, M.; Blasco, T.; Corma, A. Ammonia-containing Species Formed in Cu-chabazite as per in situ EPR, Solid-state NMR, and DFT Calculations. *J. Phys. Chem. Lett.* **2015**, *6*, 1011−1017.

(27) Godiksen, A.; Stappen, F. N.; Vennestrøm, P. N. R.; Giordanino, F.; Rasmussen, S. B.; Lundegaard, L. F.; Mossin, S. Coordination Environment of Copper Sites in Cu-CHA Zeolite Investigated by Electron Paramagnetic Resonance. *J. Phys. Chem. C* **2014**, *118*, 23126−23138.
(28) Wang, A.; Chen, Y.; Walter, E. D.; Washton, N. M.; Mei, D.; Varga, T.; Wang, Y.; Szanyi, J.; Wang, Y.; Peden, C. H. F.; Gao, F. Unraveling the Mysterious Failure of Cu/SAPO-34 Selective Catalytic Reduction Catalysts. *Nat. Commun.* **2019**, *10*, 1137.
(29) Morra, E.; Signorile, M.; Salvadori, E.; Bordiga, S.; Giamello, E.; Chiesa, M. Nature and Topology of Metal-oxygen Binding Sites in Zeolite Materials: O-17 High-resolution EPR Spectroscopy of Metal-loaded ZSM-5. *Angew. Chem., Int. Ed. Engl.* **2019**, *58*, 12398−12403.
(30) Gao, F.; Walter, E. D.; Karp, E. M.; Luo, J.; Tonkyn, R. G.; Kwak, J. H.; Szanyi, J.; Peden, C. H. F. Structure-activity Relationships in NH_3-SCR over Cu-SSZ-13 as Probed by Reaction Kinetics and EPR Studies. *J. Catal.* **2013**, *300*, 20−29.
(31) Gao, F.; Walter, E. D.; Kollar, M.; Wang, Y.; Szanyi, J.; Peden, C. H. F. Understanding Ammonia Selective Catalytic Reduction Kinetics over Cu/SSZ-13 from Motion of the Cu Ions. *J. Catal.* **2014**, *319*, 1−14.
(32) Kresse, G.; Furthmüller, J. Efficient Iterative Schemes for ab initio Total-energy Calculations Using a Plane-wave Basis Set. *Phys. Rev. B* **1996**, *54*, 11169−11186.
(33) Kresse, G.; Hafner, J. Ab initio Molecular-dynamics for Liquid-metals. *Phys. Rev. B* **1993**, *47*, 558−561.
(34) Blöchl, P. E. Projector Augmented-wave Method. *Phys. Rev. B* **1994**, *50*, 17953−17979.
(35) Perdew, J. P.; Burke, K.; Ernzerhof, M. Generalized Gradient Approximation Made Simple. *Phys. Rev. Lett.* **1996**, *77*, 3865−3868.
(36) McEwen, J.-S.; Anggara, T.; Schneider, W. F.; Kispersky, V. F.; Miller, J. T.; Delgass, W. N.; Ribeiro, F. H. Integrated Operando X-ray Absorption and DFT Characterization of Cu-SSZ-13 Exchange Sites During the Selective Catalytic Reduction of NO_x with NH_3. *Catal. Today* **2012**, *184*, 129−144.
(37) Zhang, R.; McEwen, J.-S.; Kollár, M.; Gao, F.; Wang, Y.; Szanyi, J.; Peden, C. H. F. NO Chemisorption on Cu/SSZ-13: A Comparative Study from Infrared Spectroscopy and DFT Calculations. *ACS Catal.* **2014**, *4*, 4093−4105.
(38) Jangjou, Y.; Do, Q.; Gu, Y.; Lim, L. G.; Sun, H.; Wang, D.; Kumar, A.; Li, J.; Grabow, L. C.; Epling, W. S. Nature of Cu Active Centers in Cu-SSZ-13 and Their Responses to SO_2 Exposure. *ACS Catal.* **2018**, *8*, 1325−1337.
(39) Cui, Y.; Wang, Y.; Mei, D.; Walter, E. D.; Washton, N. M.; Holladay, J. D.; Wang, Y.; Szanyi, J.; Peden, C. H. F.; Gao, F. Revisiting Effects of Alkali Metal and Alkaline Earth Co-cation Additives to Cu/SSZ-13 Selective Catalytic Reduction Catalysts. *J. Catal.* **2019**, *378*, 363−375.
(40) Gao, F.; Walter, E. D.; Washton, N. M.; Szanyi, J.; Peden, C. H. F. Synthesis and Evaluation of Cu/SAPO-34 Catalysts for NH_3-SCR 2: Solid-state Ion Exchange and One-pot Synthesis. *Appl. Catal., B* **2015**, *162*, 501−514.
(41) Martini, A.; Borfecchia, E.; Lomachenko, K. A.; Pankin, I. A.; Negri, C.; Berlier, G.; Beato, P.; Falsig, H.; Bordiga, S.; Lamberti, C. Composition-driven Cu-speciation and Reducibility in Cu-CHA Zeolite Catalysts: a Multivariate XAS/FTIR Approach to Complexity. *Chem. Sci.* **2017**, *8*, 6836−6851.
(42) Godiksen, A.; Vennestrøm, P. N. R.; Rasmussen, S. B.; Mossin, S. Identification and Quantification of Copper Sites in Zeolites by Electron Paramagnetic Resonance Spectroscopy. *Top. Catal.* **2017**, *60*, 13−29.
(43) Peisach, J.; Blumberg, W. E. Structural Implications Derived from Analysis of Electron-Paramagnetic Resonance-spectra of Natural and Artificial Copper Proteins. *Arch. Biochem. Biophys.* **1974**, *165*, 691−708.
(44) Carl, P. J.; Larsen, S. C. EPR Study of Copper-exchanged Zeolites: Effects of Correlated g- and A-strain, Si/Al Ratio, and Parent Zeolite. *J. Phys. Chem. B* **2000**, *104*, 6568−6575.
(45) Eaton, S. S.; More, K. M.; Sawant, B. M.; Eaton, G. R. Use of the EPR Half-field Transition to Determine the Interspin Distance and the Orientation of the Interspin Vector in Systems with Two Unpaired Electrons. *J. Am. Chem. Soc.* **1983**, *105*, 6560−6567.
(46) Chao, C. C.; Lunsford, J. H. EPR Study of Copper(II) Ion Pairs in Y-Type Zeolites. *J. Chem. Phys.* **1972**, *57*, 2890.
(47) Ryder, J. A.; Chakraborty, A. K.; Bell, A. T. Density Functional Theory Study of Proton Mobility in Zeolites: Proton Migration and Hydrogen Exchange in ZSM-5. *J. Phys. Chem. B* **2000**, *104*, 6998−7011.
(48) Vener, M. V.; Rozanska, X.; Sauer, J. Protonation of Water Clusters in the Cavities of Acidic Zeolites: $(H_2O)_n$·H-chabazite, n=1-4. *Phys. Chem. Chem. Phys.* **2009**, *11*, 1702−1712.
(49) Chen, P.; Rizzotto, V.; Xie, K.; Simon, U. Tracking Mobile Active Sites and Intermediates in NH_3-SCR over Zeolite Catalysts by Impedance-based in situ Spectroscopy. *React. Chem. Eng.* **2019**, *4*, 986−994.
(50) Borfecchia, E.; Negri, C.; Lomachenko, K. A.; Lamberti, C.; Janssens, T. V. W.; Berlier, G. Temperature-dependent Dynamics of NH_3-derived Cu Species in the Cu-CHA SCR Catalyst. *React. Chem. Eng.* **2019**, *4*, 1067−1080.
(51) Stoll, S.; Schweiger, A. EasySpin, a Comprehensive Software Package for Spectral Simulation and Analysis in EPR. *J. Magn. Reson.* **2006**, *178*, 42−55.
(52) Paolucci, C.; Verma, A. A.; Bates, S. A.; Kispersky, V. F.; Miller, J. T.; Gounder, R.; Delgass, W. N.; Ribeiro, F. H.; Schneider, W. F. Isolation of the Copper Redox Steps in the Standard Selective Catalytic Reduction on Cu-SSZ-13. *Angew. Chem., Int. Ed. Engl.* **2014**, *53*, 11828−11833.
(53) Zhang, Y.; Peng, Y.; Li, K.; Liu, S.; Chen, J.; Li, J.; Gao, F.; Peden, C. H. F. Using Transient FTIR Spectroscopy to Probe Active Sites and Reaction Intermediates for Selective Catalytic Reduction of NO on Cu/SSZ-13 Catalysts. *ACS Catal.* **2019**, *9*, 6137−6145.
(54) Marberger, A.; Petrov, A. W.; Steiger, P.; Elsener, M.; Kröcher, O.; Nachtegaal, M.; Ferri, D. Time-resolved Copper Speciation during Selective Catalytic Reduction of NO on Cu-SSZ-13. *Nat. Catal.* **2018**, *1*, 221−227.

https://dx.doi.org/10.1021/acscatal.0c01590
ACS Catal. 2020, 10, 9410−9419